中國機械工程學刊第三十九卷第六期第 575~583 頁(民國一百零七年)
Journal of the Chinese Society of Mechanical Engineers, Vol.39, No.6, pp 575~583 (2018)

Mechanical Char acteristics Analyses of the First Stage Impeller in the Low Pressure Cylinder of an H418 Centrifugal Compressor

Ming Zhang*, Zi-Zhen Zhao**, Meng-Li Li**, Wei-Qiang Wang*** and Hai-Bao Xie****

Keywords：Shrouded impeller, local blade thinning, mechanical characteristic, dangerous location, vibration mode.

ABSTRACT

The relevant mechanical characteristics of the first stage impeller in the low pressure cylinder of an H418 centrifugal compressor were analyzed by the finite element method. The results showed that the maximum Von Mises stress appears in the middle of the blade root when the impeller underwent only a centrifugal load. The local thinning of the blade's leading edge close to the shroud caused by wear is usually the 'small mistuning', and the natural frequencies and vibration modes of mistuned impellers are similar to that of the ideal impeller. The stress concentration mainly appeared in the middle of the blade's leading edge and the vibration mode of the blade's leading edge was similar to the bending vibration of a cantilever with a sliding mass at the other end when the impeller resonated in the region around the rated speed because of the wake flow. The research provided references for the fatigue testing of impellers in the future.

INTRODUCTION

The centrifugal compressor is the core equipment of gas deliveries used in energy, petroleum, chemical, and other important industries. High cycle fatigue (HCF) and very high cycle fatigue (VHCF) induced by the wake flow and other causes are the main failure modes of impellers which are the key components of centrifugal compressors (Cheng, 2007; Hu, 2009; Ma et al., 2011; Qi, 2004; Sivaprasad et al., 2010; Xiong, 2003). Research on the fatigue behavior and mechanism of impellers in the VHCF regime is beneficial to ensure a long operation life of centrifugal compressors. The fatigue of impellers is closely related with the impeller structure, load and other factors, so the determinations of the dangerous location and vibration mode are important to the fatigue testing of impellers. It is difficult to measure the vibration stress and strain of impellers in operation. Thus, numerical analysis of impeller mechanical characteristic is the main method to determine the dangerous location and vibration mode of impellers.

The mechanical load and the aerodynamic load are the main causes of impeller vibration. The vibration of the rotor and the vibration caused by the friction of the impeller usually appear under non-normal operating conditions, and the probabilities of occurrence are small. So only the centrifugal load is involved in the computation of mechanical load. A centrifugal compressor will be shutdown because of the protective measures against unstable air flow which usually also appears under non-normal operating conditions. The occurrence of an unstable air flow is small and the accurate calculation of unstable air flow is difficult, so the aerodynamic load under normal operating condition usually only involves the action of the wake flow (Zhou, 2013).

Small differences of geometry and material properties of an impeller caused by machining error, dynamic balancing techniques, wear in operation, and the attachment and corrosion of the working medium lead to the mistuning of an ideal impeller with periodic structures, and the mechanical characteristics

Paper Received June, 2017. Revised Sepfember, 2018. Accepted October, 2018. Author for Correspondence: Ming Zhang.
** Associate professor, School of Mechanical & Automotive Engineering, Qilu University of Technology(Shandong Academy of Sciences), Jinan, Shandong 250353, China*
*** Assistant professor, School of Mechanical & Automotive Engineering, Qilu University of Technology(Shandong Academy of Sciences), Jinan, Shandong 250353, China*
**** Professor, School of Mechanical Engineering, Shandong University, Jinan, Shandong 250061, China*
***** Undergraduate, School of Mechanical & Automotive Engineering, Qilu University of Technology(Shandong Academy of Sciences), Jinan, Shandong 250353, China*

of a mistuned impeller may be different from the ideal impeller's (Li et al., 2007; Mao et al., 2008; Zhao et al., 2012). The mistuning of an impeller in operation is mainly caused by pits, thinning, cracks, and fractures because of corrosion, wear, and fatigue. Compared with macroscopic cracks and fractures which seriously damage impellers, pits and the local thinning of the blade are more common. In this paper, the mechanical characteristics of impellers with local blade thinning are studied.

The H418 centrifugal compressor in an air compressor in the air separation unit of a large-sized nitrogenous fertilizer plant had HCF failure of the first stage impeller in the low pressure cylinder after running for half a year. The relevant mechanical characteristics of this impeller were studied using the finite element method. The dangerous location and vibration mode of the impeller were determined and which provided references for the fatigue testing of impellers in the future.

THE FINITE ELEMENT MODEL OF AN OBJECTIVE IMPELLER

The first stage impeller in the low pressure cylinder of an H418 centrifugal compressor which had HCF fracture in the blade's leading edge is the research object. The main dimensions and parameters of this impeller are as follow: diameter D=1100mm, blade number Z=19, inlet guide vane number Z_1=14, blade thickness δ=8mm, and operating speed n=5000r/min. Impeller material FV520B-I is a type of martensitic precipitation hardening stainless steel, with an elastic modulus E=194GPa, the Poisson's ratio ν=0.28, and density ρ=7820kg/m^3.

In the situation of local blade thinning caused by non-uniform wear in long-term operation, the blade's leading edge close to the shroud has a typical thinned region (Lin et al., 1994). The blade's leading edge of a similar impeller close to the shroud had local thinning as shown in Fig. 1. This region was chosen as the research location, and the effects of local blade thinning on the mechanical characteristics of the impeller were studied. The physical model of the impeller with one local thinned blade is shown in Fig. 2. Mistuning involves three types of the maximum thinned thickness (the maximum thinned thickness appears in the joint of blade's leading edge and shroud, and which is 0.3, 0.5, and 0.7 times the total blade thickness, respectively), three types of thinned blade numbers (1 or 2 or all) and two arrangements of thinned blades (adjacent or interval of one ideal blade). The different mistuning types are listed in Table 1.

Fig. 1. The local thinning of the blade's leading edge in a shrouded impeller caused by erosion.

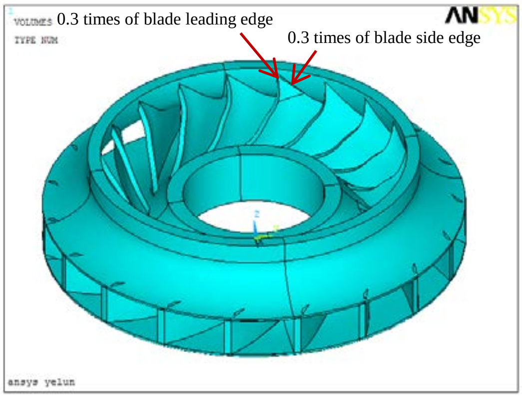

(a) The physical model of the whole impeller

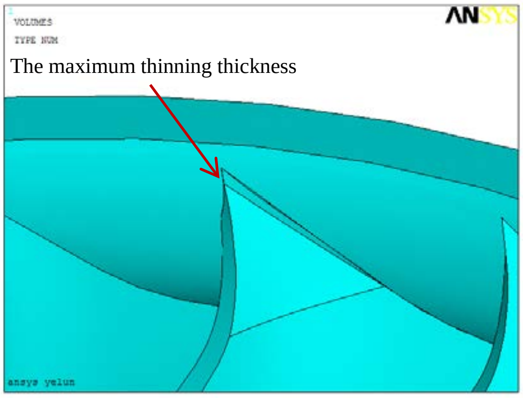

(b) Local blade thinning

Fig. 2. The physical model of impeller with one local thinned blade (the maximum thinned thickness is 0.3δ).

Table 1. Misturing numbers and mistuning types.

Number	Mistuning types
Ⅰ	Ideal impeller
Ⅱ	One blade thinned (the maximum thinned thickness is 0.3δ)
Ⅲ	One blade thinned (the maximum thinned thickness is 0.5δ)
Ⅳ	One blade thinned (the maximum thinned thickness is 0.7δ)

Ⅴ	Two adjacent blades thinned (the maximum thinned thickness is 0.3δ)
Ⅵ	Two adjacent blades thinned (the maximum thinned thickness is 0.5δ)
Ⅶ	Two adjacent blades thinned (the maximum thinned thickness is 0.7δ)
Ⅷ	Two interval blades thinned (the maximum thinned thickness is 0.3δ, interval of one ideal blade)
Ⅸ	Two interval blades thinned (the maximum thinned thickness is 0.5δ, interval of one ideal blade)
Ⅹ	Two internal blades thinned (the maximum thinned thickness is 0.7δ, interval of one ideal blade)
Ⅺ	All blades thinned (the maximum thinned thickness is 0.7δ)

The interior surface of the impeller shaft hole was fully constrained, and the size of the finite element mesh was set to 20mm after the check of mesh-size independence. The element was the tetrahedral element of SOLID187 with 10-nodes. We established the finite element mesh models of an ideal impeller and mistuned impellers, and the finite element mesh model of an ideal impeller as shown in Fig. 3.

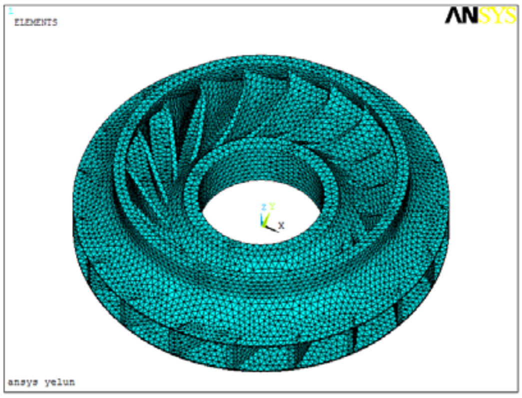

Fig. 3. The finite element mesh model of an ideal impeller.

STATIC STRESS ANALYSIS

In the static stress analysis of impellers, the effects of aerodynamic static pressure on static stress are generally ignored and only the centrifugal load is involved (Zhou, 2013). The over-speeding preload of an impeller was involved in the calculation of static stress, and the speed was first set to 5750r/min (overload 15%), then the impeller was unloaded and the speed was set to 0r/min, and the impeller was reloaded and the speed was finally set to the rated speed of 5000r/min. For the ideal impeller, the maximum Von Mises stress was 1317.23 MPa and appeared in the middle of the blade root when the impeller was over-speeding, as shown in Fig. 4. The maximum residual Von Mises stress was 233.12MPa and appeared in the joint of the blade's trailing edge and disc, as shown in Fig. 5. The maximum Von Mises stress was 996.22MPa and appeared in the middle of the blade root when the impeller operated under the rated speed, as shown in Fig. 6, and which is lower than the yield strength of FV520B-I 1030MPa (Zhou, 2013). The effects of local blade thinning on the static stress of the impeller were small. The maximum Von Mises stress of the impeller with a local blade thinned under the rated speed slightly decreased and the location of the maximum Von Mises stress was unchanged compared with the ideal impeller's. The static stress distribution of the impeller with all blades thinned is shown in Fig. 7.

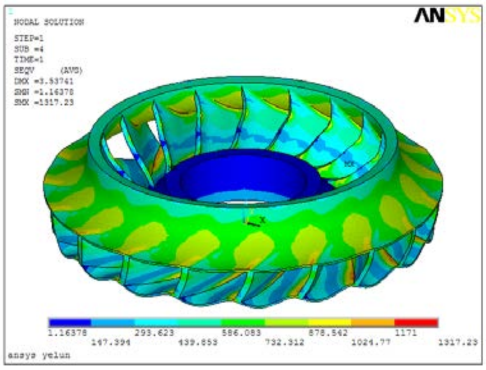

(a) The Von Mises stress of the whole impeller

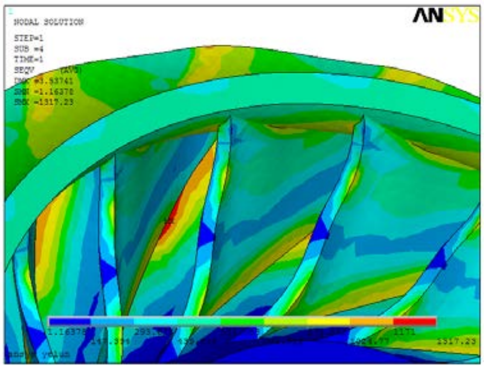

(b) The location of the maximum Von Mises stress

Fig. 4. The Von Mises stress of an ideal impeller with over-speeding.

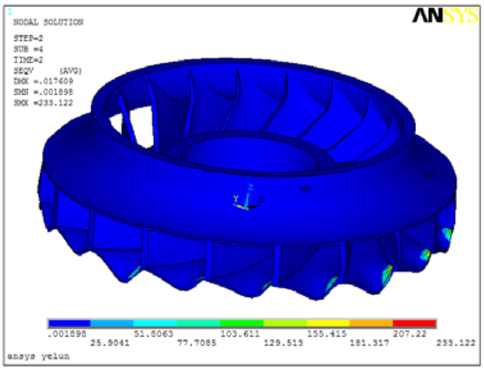

Fig. 5. The residual Von Mises stress of an ideal impeller after over-speeding.

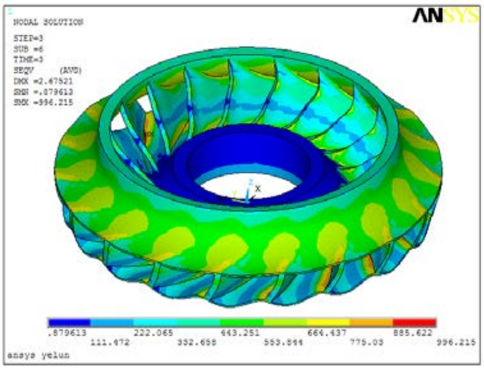

(a) The Von Mises stress of the whole impeller

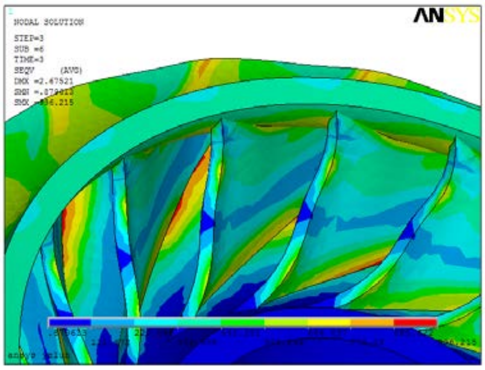

(b) The location of the maximum Von Mises stress

Fig. 6. The Von Mises stress of an ideal impeller under the rated speed.

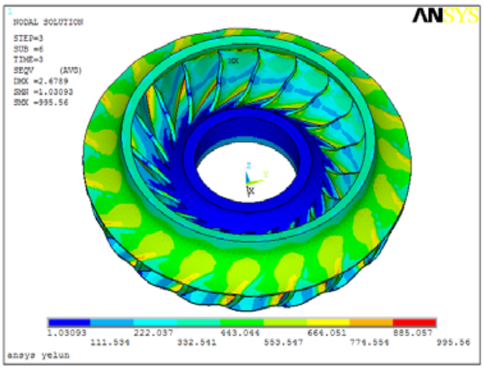

(a) The Von Mises stress of the whole impeller

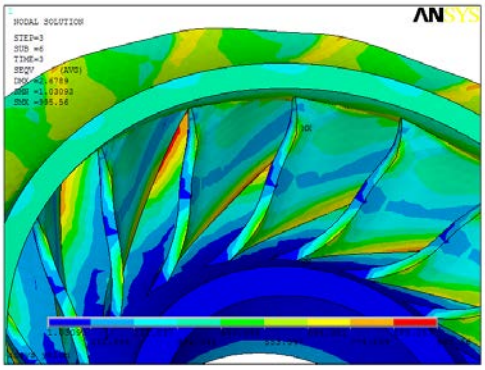

(b) The location of the maximum Von Mises stress

Fig. 7. The Von Mises stress of the impeller with all blades thinned under the rated speed.

MODAL ANALYSIS

Ideal impeller

The modal analysis results of an impeller which underwent a centrifugal load are similar to that of an impeller that did not undergo a centrifugal load, and the natural frequencies slightly increase and the vibration modes are unchanged (State Key Laboratory of Structural Analysis for Industrial Equipment, 2007). Therefore, the centrifugal load was not involved in the modal analysis of the impeller in this paper and the modal analysis was conducted using the Block Lanczos method. Also, the asymmetry caused by the uneven mesh was ignored. The minimum 30 orders of natural frequencies and vibration characteristics of an ideal impeller are shown in Table 2.

Most of the natural frequencies of an impeller are the double frequency which is the characteristic of a rotational symmetric structure. There is a frequency dense region dominated by local vibration from the 20th natural frequency to the 29th natural frequency, and there are 10 order modals in the frequency range of 32.3Hz. The pass frequency of the impeller guide vane should avoid this frequency dense region in order to reduce the possibility of resonance. The wake flow is dominated by the load with a low order frequency (Zhou, 2013), so the analysis of resonance caused by the wake flow focuses on the load with the 1st pass frequency. The 1st pass frequency $f=nZ_1/60=1166.7$Hz which is located between the 10th natural frequency and the 11th natural frequency, and the pass frequency is far smaller than the lower boundary of the frequency dense region. The difference between the pass frequency and the lower boundary of the frequency dense region is 658.6Hz, which accounts for 56.4% of the pass frequency. The rotation speed variation is about 10% when the impeller runs under normal operating condition(Zhou, 2013). Therefore, the impeller does not resonate in the frequency dense region in a normal situation.

Table 2. The minimum 30 orders of natural frequencies and vibration characteristics of an ideal impeller.

Modal order	Natural frequency /Hz	Vibration characteristic
1	443.21	Whole
2	443.25	Whole
3	456.15	Whole
4	456.18	Whole
5	563.19	Whole
6	825.52	Whole
7	825.57	Whole
8	891.98	Whole
9	1144.6	Whole
10	1144.7	Whole
11	1287.4	Whole
12	1287.5	Whole
13	1401.3	Whole
14	1401.5	Whole
15	1614.1	Whole
16	1614.2	Whole
17	1704.4	Local dominated
18	1704.6	Local dominated
19	1796.9	Whole
20	1825.3	Local dominated
21	1826.3	Local dominated
22	1831.7	Local
23	1832.4	Local
24	1833.3	Local
25	1833.5	Local
26	1843.5	Local
27	1849.2	Local
28	1856.8	Local
29	1857.6	Local
30	1902.8	Local

The modal stresses of an ideal impeller when the speed of the impeller is close to the rated speed are shown in Fig. 8. The stress concentration mainly appears in the middle of the blade's leading edge and this location is in accordance with the fatigue fracture site of this impeller mentioned in the literature (State Key Laboratory of Structural Analysis for Industrial Equipment, 2007). According to Newton's second law, the equations of motion for the tank vehicle can be expressed in terms of the moving *X*, *Y* coordinates as follows:

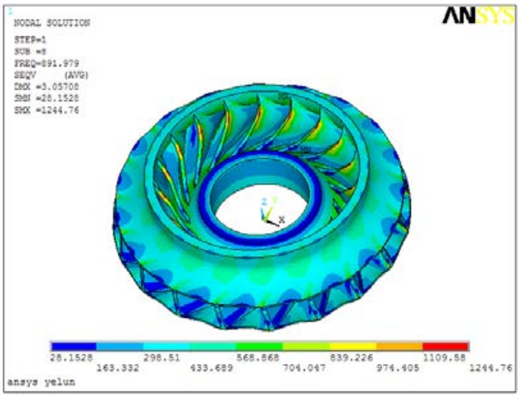

(a)The 8th natural frequency 891.98Hz

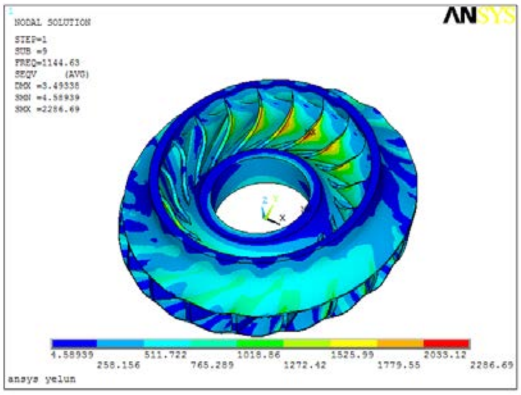

(b) The 9th natural frequency 1144.63Hz

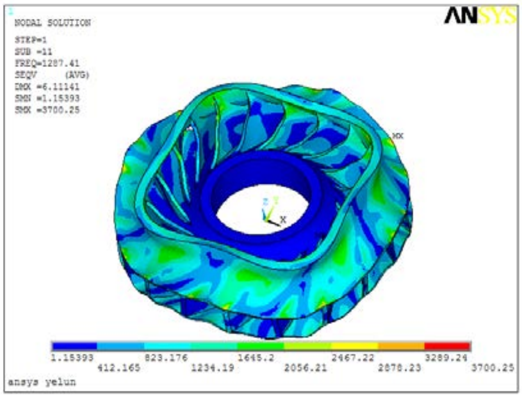

(c) The 11th natural frequency 1287.41Hz

Fig. 8. The modal stresses of an ideal impeller when the impeller speed is close to the rated speed.

Mistuned impellers

Considering the local thinning of the blade's leading edge close to the shroud in section 2, the modal analyses of mistuned impellers were carried out. The natural frequencies of different mistuned impellers were compared with the ideal impeller's as shown in Table 3 and Table 4.

Table 3. Comparison of natural frequencies between different mistuned impellers (Hz).

Order	Ⅰ	Ⅱ	Ⅲ	Ⅳ	Ⅴ

1	443.21	443.22	443.2	443.19	443.22
2	443.25	443.27	443.28	443.28	443.28
3	456.15	456.15	456.18	456.17	456.18
4	456.18	456.2	456.2	456.24	456.2
5	563.19	563.19	563.21	563.19	563.21
6	825.52	825.34	825.27	825.06	825.29
7	825.57	825.53	825.53	825.56	825.48
8	891.98	891.97	891.98	891.94	891.96
9	1144.6	1144.7	1144.7	1144.6	1144.7
10	1144.7	1144.8	1144.8	1144.9	1144.8
11	1287.4	1287	1286.8	1286.4	1287
12	1287.5	1287.4	1287.4	1287.4	1287.2
13	1401.3	1401.4	1401.4	1401.5	1401.5
14	1401.5	1401.6	1401.7	1401.6	1401.7
15	1614.1	1614.2	1614.1	1614	1614.2
16	1614.2	1614.4	1614.5	1614.5	1614.4
17	1704.4	1704	1703.8	1703.2	1703.9
18	1704.6	1704.2	1704.5	1704.4	1704.1
19	1796.9	1796.8	1796.9	1796.8	1796.8
20	1825.3	1824.5	1826.1	1825.4	1824.9
21	1826.3	1826.2	1827	1826.8	1826.9
22	1831.7	1830.8	1831.8	1830.7	1831.3
23	1832.4	1832.4	1832.3	1832.8	1832.4
24	1833.3	1833.1	1834	1833.3	1833.2
25	1833.5	1833.7	1834.5	1834.4	1834.3
26	1843.5	1843.1	1844.4	1843.9	1844.1
27	1849.2	1848.9	1850.3	1849.5	1849
28	1856.8	1856.2	1857.7	1856.8	1856.9
29	1857.6	1857.3	1858.8	1858.2	1857.6
30	1902.8	1902.5	1903.4	1902.7	1902.5

Table 4. Comparison of natural frequencies between different mistuned impellers (Hz).

Order	Ⅵ	Ⅶ	Ⅷ	Ⅸ	Ⅹ	Ⅺ
1	443.18	443.12	443.22	443.21	443.14	442.74
2	443.28	443.31	443.27	443.29	443.28	442.82
3	456.18	456.17	456.16	456.2	456.21	456.45
4	456.24	456.27	456.22	456.23	456.23	456.49
5	563.2	563.16	563.19	563.21	563.16	562.48
6	825.1	824.77	825.31	825.12	824.93	820.83
7	825.42	825.34	825.42	825.37	825.28	821.63
8	891.94	891.88	891.95	891.93	891.87	890.77
9	1144.7	1144.6	1144.7	1144.7	1144.6	1145.3
10	1144.9	1145	1144.8	1144.9	1145	1145.7
11	1286.6	1286	1286.8	1286.2	1285.6	1276.8
12	1286.9	1286.6	1287.3	1287.3	1287.2	1277.9
13	1401.5	1401.5	1401.4	1401.5	1401.5	1402.8
14	1401.7	1401.8	1401.7	1401.8	1401.8	1403.1
15	1614.1	1613.9	1614.2	1614.2	1614	1613.6
16	1614.4	1614.5	1614.3	1614.4	1614.4	1614
17	1703.6	1702.8	1703.6	1702.8	1702	1690.1
18	1703.7	1703.2	1704.2	1704.3	1704.3	1691.8
19	1796.9	1796.8	1796.8	1796.8	1796.9	1796.8
20	1825.7	1825.2	1824.9	1825.6	1825	1823.9
21	1827.1	1827	1826.5	1826.6	1826.8	1824.8
22	1831.2	1830.9	1831	1830.9	1830.4	1827.2
23	1832.5	1832	1832.3	1832.5	1832.3	1827.6
24	1833.4	1833.4	1832.9	1833.2	1833.1	1832.2
25	1834.6	1834.3	1834.4	1834.4	1834.6	1833.4
26	1844.1	1844.2	1843.8	1843.9	1844	1843.4
27	1849.8	1849.4	1849	1849.5	1849.3	1848.8
28	1857.2	1857.5	1856.6	1857.4	1857	1856.6
29	1858.5	1857.7	1857.6	1857.8	1857.9	1856.9
30	1902.9	1902	1902.7	1902.6	1902.2	1896.6

In Table 3 and Table 4, the natural frequencies of most mistuned impellers were almost unchanged compared with the ideal impeller's although the maximum thinned thickness of blade was up to 0.7 times the total blade thickness. Some natural frequencies of the impeller with all blades thinned slightly changed due to larger mistuning. The vibration modes of different impellers were identical. The 9th vibration modes of some impellers are shown in Fig. 9. It was because the local blade thinning caused by wear was generally the 'small mistuning', and the topology structures of different impellers were essentially identical. So the natural frequencies and vibration modes of mistuned impellers seemed unchanged compared with the ideal impeller's.

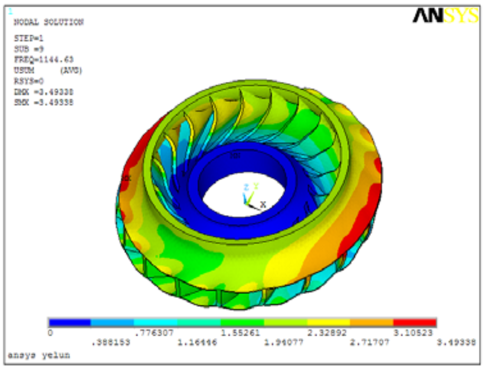

(a) Ideal impeller

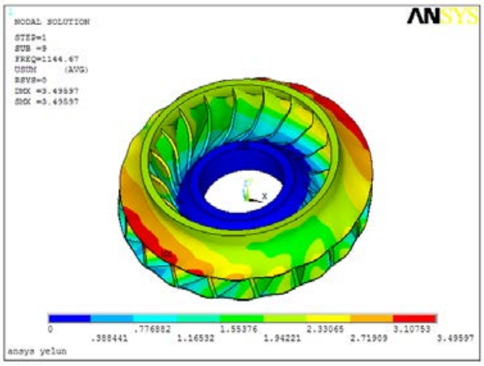

(b) The mistuned impeller of Ⅷ type

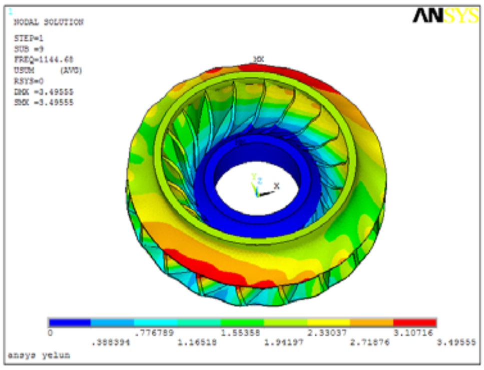

(c)The mistuned impeller of Ⅸ type

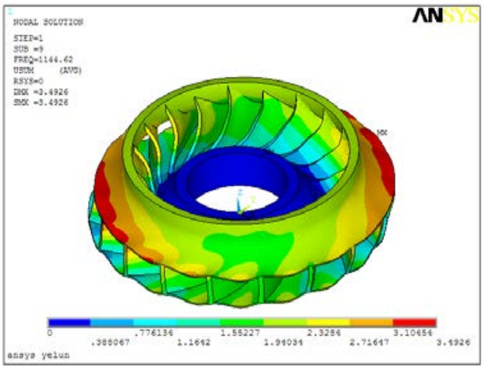

(d) The mistuned impeller of Ⅹ type

Fig. 9. The 9th vibration modes of some impellers.

THE HARMONIC RESPONSE ANALYSIS OF THE WAKE FLOW

The dynamic response of the impeller under the action of the wake flow was simulated through harmonic response analysis, and the stress amplitude and distribution were obtained. The accurate calculation of fluctuating pressure on the blade was difficult in the unsteady CFD calculation, but the calculation of the static pressure was relatively simple with high accuracy. The fluctuating pressure can be estimated as 5% of the static pressure in engineering (Zhou, 2013). The static pressure of this impeller under normal operating condition is about 13,950Pa (Guan et al., 2012), and then the amplitude of the fluctuating pressure is about 700Pa. The harmonic pressure is applied on the pressure surface of each blade. The pressure amplitude is 700Pa, and the initial phase angle is 0 radians. The phase difference between adjacent blades is involved, and the damping coefficient is 0.0005. Assuming that the excitation frequency is equal to the natural frequency of the impeller close to 1166.7Hz, the dynamic stress caused by impeller resonance when the impeller is under the action of the wake flow is as shown in Fig. 10.

Fig. 10 shows that the resonance happened when the frequency of the wake flow was equal to the 8th natural frequency 891.98Hz, and the resonance could not happen when the frequency of the wake flow was equal to the 9th to 12th natural frequency. In fact, when the excitation frequency and the load distribution were both in accordance with the natural frequency and vibration mode of the impeller, the impeller resonated. Only when the excitation frequency was equal to the natural frequency of the impeller and the impeller did not resonated. When the frequency of the wake flow was equal to the 8th natural frequency 891.98Hz, the maximum Von Mises stress amplitude of impeller was 33.3MPa and appeared in the middle of the blade’s leading edge.

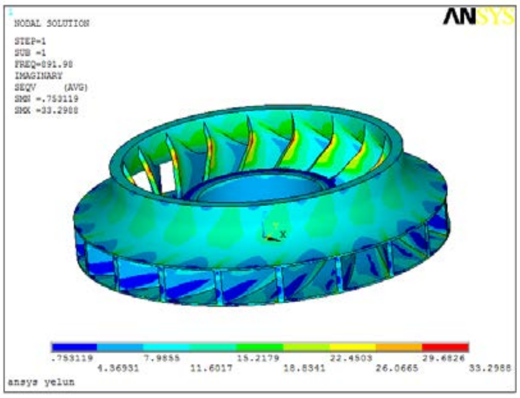

(a) The excitation frequency is equal to the 8th natural frequency 891.98Hz

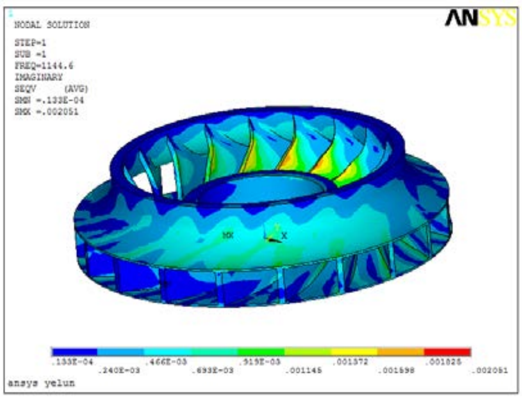

(b) The excitation frequency is equal to the 9th natural frequency 1144.63Hz

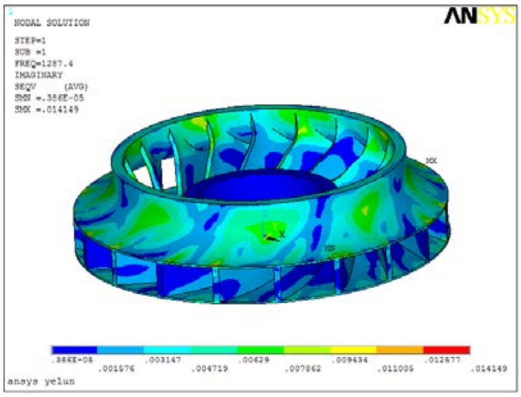

(c) The excitation frequency is equal to the 11th natural frequency 1287.41Hz

Fig. 10. The dynamic stress amplitude of the impeller caused by wake flow in a normal operating situation.

Based on the previous modal analysis, the modal displacement of the blade's leading edge when the excitation frequency is equal to the 8th natural frequency 891.98Hz was studied. The selected path is shown in Fig. 11, and the total modal displacements (U_{sum}) and the circumferential modal displacements (U_{φ}) of 14 nodes on the path are shown in Fig. 12. The maximum displacement appeared in the joint of the blade's leading edge and shroud. The displacement gradually decreased as the location on the blade's leading edge moved closer to the disc, and the displacement was almost equal to zero in the joint of the blade's leading edge and disc. The displacement differences of the node close to the shroud were relatively small, so the vibration mode of the blade's leading edge was similar to the bending vibration of a cantilever with a sliding mass at the other end.

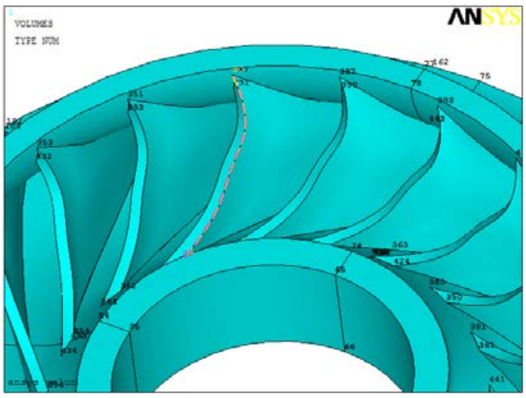

Fig. 11. The selected path of the blade's leading edge.

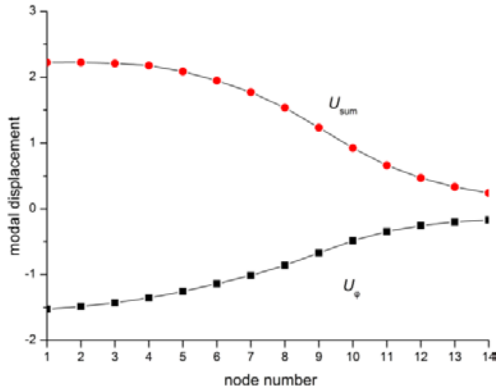

Fig. 12. The modal displacement of the selected path of the blade's leading edge.

CONCLUSIONS

The relevant mechanical characteristics of the first stage impeller in the low pressure cylinder of an H418 centrifugal compressor were analyzed. The research provided references for the fatigue testing of impellers in the future. It can be concluded that:

(1) The maximum static stress appeared in the middle of the blade root when the impeller underwent only a centrifugal load.

(2) The local thinning of the blade's leading edge close to the shroud caused by wear could not change the topological structures of the impeller, and the natural frequencies and vibration modes of mistuned impellers seemed to changed very little compared with that of an ideal impeller.

(3) The dangerous location was the middle of the blade's leading edge and the maximum stress amplitude was 33.3MPa when the impeller resonated in the region around the rated speed because of the wake flow, and the dangerous location was in accordance with the fatigue fracture site.

(4) The vibration mode of a selected path of the blade's leading edge was similar to the bending vibration of a cantilever with a sliding mass at the other end.

ACKNOWLEDGEMENTS

The authors gratefully acknowledge the financial support provided by National Natural Science Foundation of China (Grant No. 51705265). Thanks to Prof. Zhang Zhao, Dalian University of Technology, for the initial physical model of the impeller and relevant technical reports. Thanks to Dr. Edward C. Mignot, Shandong University, for linguistic advice.

REFERENCES

Cheng D.K., "The fracture reason analysis and repair of rotor blade in nitric oxide compressor," Compressor Blower & Fan Technology, No. 04, pp. 46-48+51 (2007).

Guan Z., Wang Y., Yang S., et al., "Analyses of dynamic characteristics of enclosed impeller of large centrifugal compressor," Journal of dalian university of technology, Vol.52, No. 3, pp. 320-326 (2012).

Hu S.Z., "Analysis of cracking causes of impeller of rich gas compressor and countermeasure," Corrosion & Protection in Petrochemical Industry, No. S1, pp. 63-68 (2009).

Li S.T., Xu Q.Y., "Fluid induced vibration and dynamic fatigue in centrifugal impeller," Chinese Journal of Applied Mechanics, No. 03, pp. 353-358+500 (2007).

Lin J., Liang X., Zhao B., "Study on the Wear Characteristics of the Centrifugal Impellers with Gas-solid Two-phase Flow," Fluid Machinery, No. 01, pp. 12-16+64 (1994).

Ma X.M., Hu L.X., "Failure analysis on fracture of impeller blades of high-speed centrifugal aircompressor," Physical Testing and Chemical Analysis Part A(Physical Testing), No. 08, pp. 527-530+533 (2011).

Mao Y.J., Qi D.T., Xu Q.Y., "Numerical study on high cycle fatigue failure of a centrifugal compressor impeller blades," Journal of Xi'an Jiaotong University, No. 11, pp. 1336-1339 (2008).

Qi W., "The solution of a compressor blade fracture accident," General Machinery, No. 05, pp. 64-67 (2004).

State Key Laboratory of Structural Analysis for Industrial Equipment, The Reliability Study of Impeller of Large Centrifugal Compressor (2007).

Sivaprasad S., Narasaiah N., Das S.K., et al., "Investigation on the failure of air compressor," Engineering Failure Analysis, Vol.17, No. 1, pp. 150-157 (2010).

Xiong X.L., "The accident reason and treatment measure of a centrifugal compressor impeller "; Chemical Equipment & Anticorrosion, No. 04, pp. 23-24 (2003).

Zhao W.Y., Zhang J.Z., Zhou C.W., "Study on the vibration localization in the centrifugal Impeller with periodic structures," Chinese Journal of Applied Mechanics, No. 06, pp. 699-704+775 (2012).

Zhou M., "Fatigue Analysis of Impeller of Large Centrifugal Compressors,"; M.D. Thesis, School of Mechanical Engineering, Dalian University of Technology, Dalian, China (2013).

NOMENCLATURE

D	Impeller diameter (mm)
E	Elastic modulus (GPa)
f	Frequency (Hz)
n	Operating speed (r/min)
U_{sum}	Total modal displacements
U_{φ}	Circumferential modal displacements
Z	Blade number
Z_1	Inlet guide vane number
δ	Blade thickness (mm)
v	Poisson's ratio
ρ	Density (kg/m^3)

H418 離心壓縮機低壓缸一級葉輪力學特性分析

張明 趙姿貞 李夢麗 王威強 解海寶
齊魯工業大學（山東省科學院）機械與汽車工程學院
山東大學機械工程學院

摘要

作者應用有限單元法，對某離心壓縮機閉式葉輪及磨損致葉片前緣近蓋盤處局部減薄的該葉輪進行了相關力學特性分析。研究發現，在離心載荷的作用下最大應力出現在葉根中部；葉輪在尾流激振的作用下發生共振時，應力集中主要出現在葉片前緣中部；磨損導致的葉片前緣近蓋盤處的局部減薄通常為“小失諧”，失諧葉輪固有頻率和各階振型與諧調葉輪相似；進一步界定了尾流激振導致葉輪共振時的危險部位及振動形式，為後續真實葉輪的疲勞試驗提供了指導。